International Journal of Thermal Sciences 49 (2010) 1095–1102

Contents lists available at ScienceDirect

International Journal of Thermal Sciences

journal homepage: www.elsevier.com/locate/ijts

An investigation of the phonon properties of silicon nanowires

Mei-Jiau Huang*, Chieu-Chou Weng, Tai-Ming Chang

Department of Mechanical Engineering, National Taiwan University, Taipei, Taiwan, ROC

ARTICLE INFO

Article history:
Received 3 September 2009
Received in revised form
4 February 2010
Accepted 4 February 2010
Available online 11 March 2010

Keywords:
Silicon nanowires
Molecular dynamics simulations
Confined phonon spectrum

ABSTRACT

The phonon dispersion relations and density of states under the size confinement effect are crucial in order either to obtain accurate solutions of the phonon Boltzmann transport equation or to obtain properly quantum-corrected temperatures for low-dimensional materials. This work draws the confined phonon properties of silicon nanowires from the equilibrium molecular dynamics simulations. The simulation results show discrete acoustic phonon modes with smaller group velocities and many additional modes in the region of large wave numbers and small frequencies, compared to the continuous bulk counterparts. The latter shifts the distribution of phonon density of states toward the lower frequency. The lattice thermal conductivities of infinitely long silicon wires of diameter 4.1 nm, 7.6 nm, and 10.6 nm are next calculated using the non-equilibrium molecular dynamics simulations, with temperatures properly quantum corrected based on the confined phonon density of states. The lattice thermal conductivities are found to be significantly smaller than the bulk value and depend only weakly on the temperature, implying that the surface scattering strongly dominates over the phonon–phonon interaction.

1. Introduction

In the past two decades, lot of attention has been paid to the low-dimensional materials because of the demand for miniaturization of electronic devices and the desired thermal as well as electric properties for thermoelectric applications [1–3]. It was realized that low-dimensional materials can possibly result in a higher power factor because of the size-quantization effects and electron energy filtering [4,5] and in a lower thermal conductivity [6–8] as the lattice waves are confined when the characteristic length scale of the materials is smaller than or comparable to the phonon mean free path. Among all, the differences in the thermoelectric properties between nanowires and bulk materials are expected to be most substantial due to the large surface-to-volume ratio of nanowires.

Nanowires are usually prepared in some porous host materials [9–12]. Experimental measurements of the electric resistance of the bismuth-in-alumina nanocomposites confirmed the metal-to-semiconductor transition at a wire diameter about 49 nm [9] and a significant increase in the Seebeck coefficient when the diameter is 9 nm [10]. Lee et al. [11] found the composition of Bi–Te nanowires can be controlled by the electrodeposition method and the relaxation time in the pulsed electrodeposition approach. Lin et al. [12] proposed the trigonal axis is the most favorable wire orientation for thermoelectric applications based on the band structure of Bi nanowires and a semiclassical transport model. The thermal conductivity of individual single crystalline intrinsic Si nanowire was measured and found to be lower than the bulk value by at least two orders of magnitude [13]. The prototype thermoelectric device fabricated by Abramson et al. (2004) [14] comprised of arrays of silicon nanowires embedded in a polymer matrix. Seol et al. [15] employed the electron beam lithography to measure the thermopower and electrical conductivity of an individual InSb nanowire grown using a vapor-liquid-solid method (VLS). The measurements revealed low Seebeck coefficient and high electrical conductivity compared to those for pure bulk InSb crystals.

While Hicks and Dresselhaus [4,5] proposed using the characteristic length scale of the materials as a new design parameter for a high power factor, the increase in the figure-of-merit of the low-dimensional materials is mainly attributed to the large reduction in the thermal conductivity. Theoretical models for the thermal conductivity of low-dimensional semiconductors are mostly built on the phonon Boltzmann transport equation (PBTE) under the single-relaxation-time approximation and experimentally measured or theoretically calculated phonon dispersion relations. Analytical solutions [7,8,16–18] and Monte-Carlo solutions [19–22] were both attempted. The phonon dispersion relations of low-dimensional materials are nonetheless different from the bulk ones due to the size confinement effect and are very hard to measure. Those predicted according to the continuous elastic models

* Corresponding author.
E-mail address: mjhuang@ntu.edu.tw (M.-J. Huang).

1290-0729/$ – see front matter © 2010 Elsevier Masson SAS. All rights reserved.
doi:10.1016/j.ijthermalsci.2010.02.002

Nomenclature

A	cross-sectional area of the nanowire, nm^2
$D(\omega)$	phonon density of states, fs
$\vec{e}_q$	polarization direction
$\hbar$	reduced Planck constant, $1.054571628 \times 10^{-34}$ J s
k	thermal conductivity, W/m K
k_B	Boltzmann constant, $1.3806503 \times 10^{-23}$ J/K
L_z	nanowire length, nm
$\vec{l}_i$	position of lattice point, nm
N	total number of atoms in the system
n	equilibrium phonon distribution
$\vec{q}$	phonon wave vector, 1/nm
$\vec{r}_i$	position of atom i, nm
T	temperature, K
T_{MD}	classical temperature, K
t	time, fs
$\vec{v}_i$	velocity of the atom i, nm/ps
x,y,z	cartesian coordinates, nm
$\bar{x},\bar{y}$	location of wire axis, nm

Greek symbols

α_q	normal coordinate, nm
$\Delta\varepsilon$	amount of energy injected at every time step, meV
Δt	time increment, fs
δ	width of source/sink region, nm
θ_{Debye}	Debye temperature, K
ω	phonon frequency, 1/fs
ω_D	Debye frequency, 1/fs
σ	characteristic length associated with the two-body potential, nm

[6–8,16] are incapable of capturing the phonon behaviors near the boundary of the Brillouin zone. Besides, the elastic models are isotropic and thus useful only for crystalline materials. To improve the accuracy of the PBTE solutions, the actual confined phonon spectra must be incorporated. And this constitutes the motivation of this work.

The phonon properties of low-dimensional materials can be best compassed via the molecular dynamics simulations (MD). Given a proper interatomic potential and the initial positions and velocities of atoms, MD traces the atomic trajectories by Newton's second law. Phonon dispersion relations and the phonon density of states are obtainable by measuring the vibrational motion of atoms from an equilibrium system and taking advantage of Fourier transforms [23]. In addition to ameliorating the PBTE solutions, these confined phonon spectra are also relevant for interpreting the MD simulation results. Traditionally, one defines the temperature (T_{MD}) by equating it to the average atomic kinetic energy divided by $3k_B/2$, where k_B is the Boltzmann constant. This definition fails nonetheless when the temperature is not high enough (below the Debye temperature θ_{Debye}) to allow all vibrational modes excited. A quantum correction [14,24–26] thus becomes necessary, which demands the information of the confined phonon density of states.

The thermal conductivity on the other hand can be calculated either via the Green-Kubo relation measured from an equilibrium MD (EMD) simulation or based on the Fourier's conduction law and the measured temperature gradient and heat flux from a non-equilibrium MD (NEMD) simulation. A comparison between these two approaches can be found in the work of Schelling et al. [27]. To imitate a real system that possesses temperature gradients, we choose NEMD for calculating the thermal conductivity in the present study.

In this work, we thus intend to apply the EMD approach to obtain the confined phonon spectra and apply the NEMD approach to study the axial thermal conductivity of silicon nanowires. The Stillinger–Weber (SW) interatomic potential is adopted. To speed up the computations, a parallel simulation code taking advantage of the spatial-decomposition technique [28] is developed.

2. Computational methodology

The MD simulations start from a selection of a suitable potential function to describe the interaction among atoms. Several potential models have been developed for silicon in the literatures such as Stillinger–Weber (SW) potential, Tersoff potential, and modified embedded atoms methods (MEAM). Heino [29] employed MEAM for silicon thin films. His calculations of the dispersion relations of bulk silicon didn't agree well with the inelastic-neutron-scattering measurements [30], except for long acoustic phonons. In this study we adopt the SW potential because it can accurately predict experimental measurements of bulk dispersion relations, specific heats, thermal expansion coefficient, the elastic constants and melting temperature [27]. The SW potential contains two- and three-body potentials to maintain the diamond structure of silicon. The involved parametric values used herein are all extracted from the work of Schelling et al. (2002) [27].

2.1. EMD and NEMD approaches

Fig. 1 is a schematic diagram of the simulated nanowire, which has an approximately octagonal cross section and a length of L_z in the z [100] direction. Periodic boundary conditions are imposed in the z direction and the surface of the nanowire is free. The time marching is executed via the velocity-verlet method. In an EMD simulation, the system is initially set at $T_{MD} = 300$ K with a Maxwell–Boltzmann velocity distribution. The simulation is first run for 30 ps by enforcing the system temperature at 300 K using the velocity rescaling technique and then for another 30 ps for the system to reach new equilibrium after the velocity rescaling is turned off. The time period 30 ps is chosen to ensure the current autocorrelation coefficient [27] and the velocity autocorrelation coefficient [23] have both dropped below 1%. The system thus reaches its thermal equilibrium at the prescribed temperature ($T_{MD} = 300$ K) and statistic samples are not collected until now.

To generate a constant heat flux in the system (a non-equilibrium system), we adopt the velocity-rescaling algorithm suggested by Jund et al. [31]. As shown in Fig. 1, an amount of heat $\Delta\varepsilon$ is added into the region of thickness δ(chosen to be 1.2 nm in this study) centered at $z = L_z/4$ (source region) and removed from the region of same thickness centered at $z = 3L_z/4$ (sink region) at every simulation time step. The system is divided into slices along the z direction, each having a thickness of 1/4 lattice constant (about 0.14 nm). When the system achieves stationary, a local equilibrium is also assumed within each slice. The classical temperature is then calculated based on the temporal average kinetic energy of atoms within each slice. A quantum correction in a way to be described later follows immediately. The thermal conductivity is finally calculated based on the ratio of the temperature gradient and the

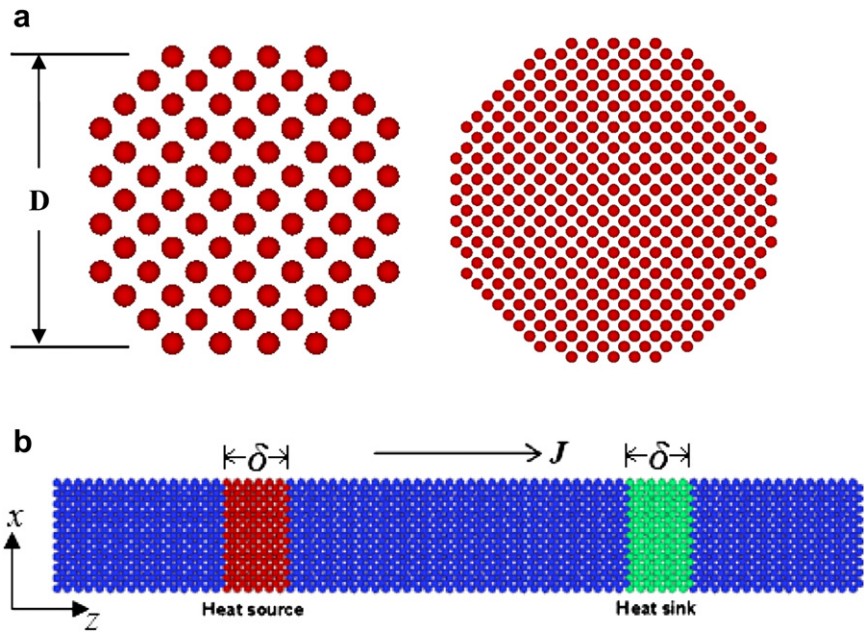

Fig. 1. (a) An illustration of the cross sections of the simulated nanowires (diameter D ≈ 1.6 nm and 4.1 nm); (b) a schematic diagram of the NEMD simulation.

heat current $\Delta\varepsilon/(2A\Delta t)$, where Δt is the time step and A is the cross-sectional area of the silicon wire.

2.2. Parallel computation

To speed up the calculation of interatomic forces, the Verlet list and the cell link techniques are both employed herein [32]. Moreover, the tremendously large computational amount is overcome by developing a spatial-decomposition parallel code. Because atoms in the solids vibrate only in the neighborhood of their equilibrium positions, we assign a fixed region of atoms to one processor for calculation. Data that must be communicated between neighboring processors is estimated to be within a distance slightly greater than the maximum displacement of atoms. Shown in Fig. 2 is a two-dimensional example. The communication is finished by sequentially transferring/receiving data within the prescribed range to/from the neighboring processors. Our simulation results show a prescribed range of thickness 1.5σ, 2.6σ, and 5σ is sufficiently wide for bulk, thin film, and wire cases respectively up to 700 K, where σ is the characteristic length associated with the two-body potential.

2.3. Confined phonon spectra and density of states

There are many existing methods for calculating the phonon dispersion relations, such as by measuring the autocorrelation function of atomic velocity [29], of the displacement of atomic vibration [33], or of the atomic position [23]. The first method takes a much longer time to converge and the other two perform similarly. In the present work, we adopt the last method for simplicity. In this method, the Fourier transform of the normal coordinate calculated as

$$\alpha_q(t) = \sum_i \vec{r}_i(t)\cdot\vec{e}_q\cos(\vec{q}\cdot\vec{l}_i) \tag{1}$$

is desired, where $\vec{r}_i$ is the instantaneous position of atom i, $\vec{e}_q$ is the polarization direction, $\vec{l}_i$ is the position of the lattice point, and $\vec{q}$ is the associated wave vector. It can be shown that the relative Fourier amplitude of the corresponding characteristic frequency increases linearly with the simulation time; in other words, the characteristic frequency becomes more and more apparent as the simulation time increases [34]. After the system reaches equilibrium, the position of one of the two atoms in a basis is averaged for 100,000 time steps ($\Delta t = 0.3$fs) and the result is taken as the lattice point of this basis. The normal coordinate is then calculated for every 24fs and a total of 25,000 samples are taken (the highest and the lowest resolved frequencies are thus 20.8THz and 1.6GHz respectively).

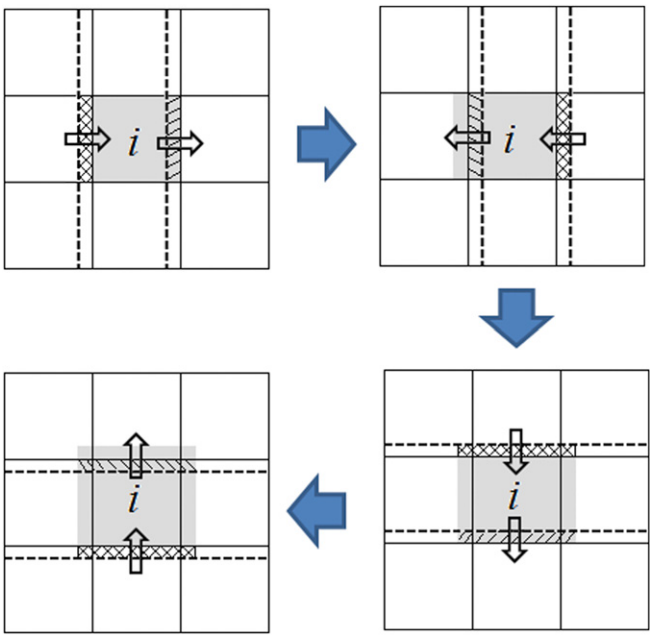

Fig. 2. An illustration of the two-dimensional data communication of the processor i with its neighbors. The grey region indicates the data the processor i owns. The crossed and slashed regions are the data the processor is going to receive and transfer respectively.

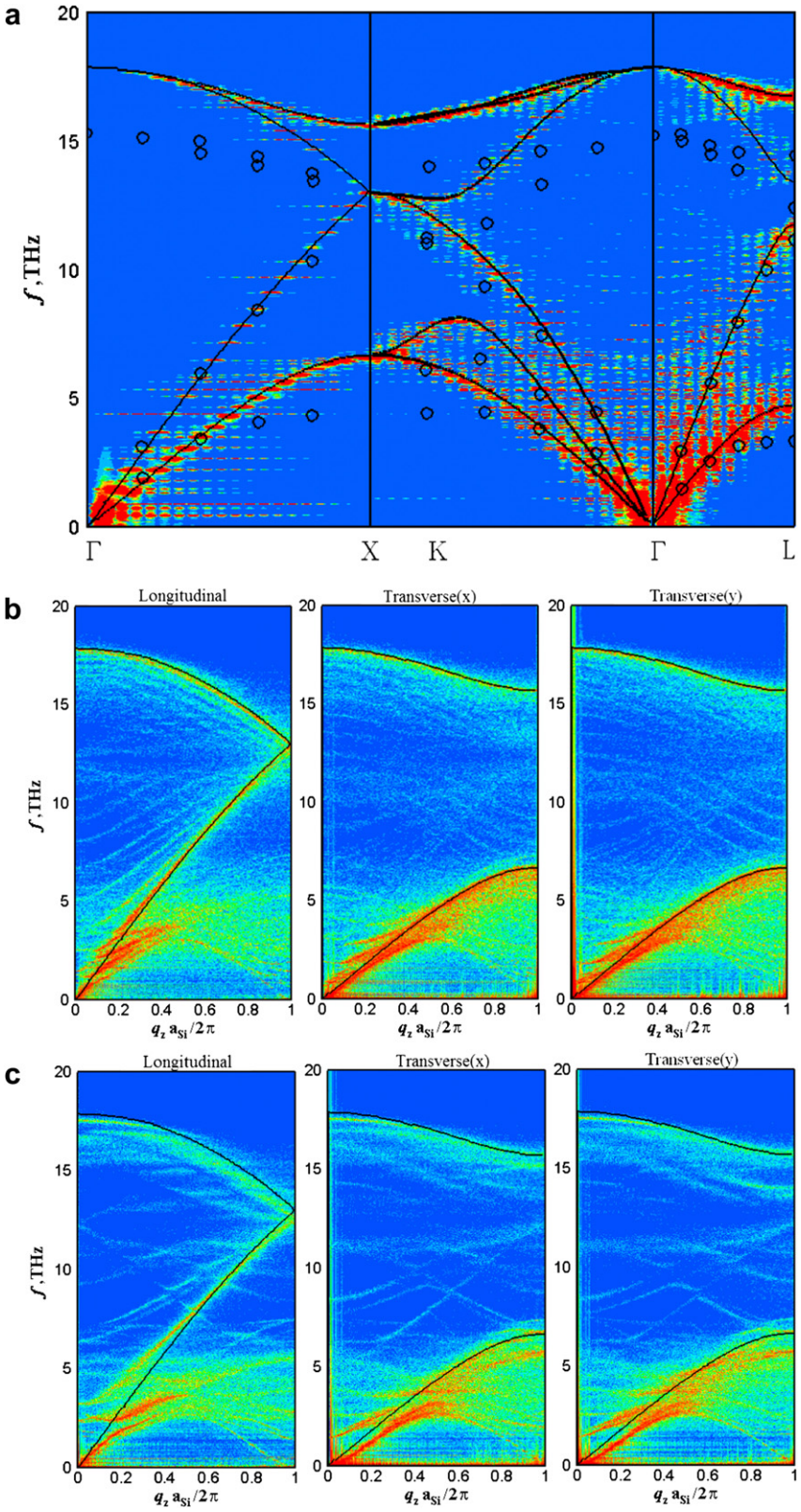

Fig. 3. The phonon spectra of bulk silicon (a) and silicon wires of diameter 4.1 nm (b) and 1.6 nm (c).

The phonon density of states, $D(\omega)$, on the other hand is obtained by measuring the velocity autocorrelation function and taking a cosine Fourier transform [23,33], namely

$$D(\omega) = 6N \int_0^\infty \left\langle \sum_i \vec{v}_i(t+\tau)\cdot\vec{v}_i(\tau) \right\rangle \cos(\omega t)dt \Big/ \pi \left\langle \sum_i |\vec{v}_i|^2(\tau) \right\rangle \tag{2}$$

where $\vec{v}_i$ is the velocity of the atom i, N is the total number of atoms in the system, ω is the phonon frequency, and the angular bracket represents a temporal average. The correlation value is calculated for every 3 fs and for a total time period of 3 ps. The time integration is done by using the fourth-order Simpson method.

3. Results and discussions

3.1. Confined phonon spectra

Shown in Fig. 3 are the calculated spectra of bulk silicon and silicon wires of diameter 4.1 nm and 1.6 nm and of length 54 nm and 109 nm at $T_{MD,i} = 300$ K. For the bulk dispersion relations, the system size is 10 nm × 10 nm × 10 nm and periodic boundaries are used in all three directions. It is seen the simulated bulk spectra agree very well with the lattice-dynamics calculation [35] and with the experimental measurement [36,37]. The only difference appears in the slightly higher frequencies of the simulated optical phonons and the acoustic phonons near the boundary of the Brillouin zone, which are both minor for heat conduction due to their much smaller group velocities. This confirms the accuracy and reliability of the employed SW potential and related parametric values.

Also shown in Fig. 3 are the longitudinal and transverse dispersion relations of the silicon wires along the [100] direction. The optical branches differ little from the bulk counterparts (black curves) but seemingly become thicker. Given a wave number, several peaks are found for the acoustic phonons on the other hand; the thinner the wire, the larger the frequency gaps are. In addition, the phonon group velocities of these confined acoustic phonon modes are obviously much smaller than those of the unconfined (bulk) ones, particularly at low wave numbers which dominate the heat conduction in the bulk materials. Furthermore, it is observed many phonons populate in the region of large wave numbers and small frequencies, with small or even negative group velocities. These confinement characteristics all lead to a reduction of the thermal conductivity.

Fig. 4 shows the calculated phonon density of states of the silicon wires, compared with the bulk one and that of a silicon thin film of thickness 4.2 nm. It is seen the peak corresponding to the optical branch (about 16–17 THz) decreases with decreasing wire thickness as well as decreasing dimension, compensated by a rising dip at the frequency ≈ 15THz. The acoustic phonon modes also shift toward lower frequencies as the wire thickness or the dimension decreases. This must correlate with the phonon modes observed in the high-wave-number-and-low-frequency region as mentioned above. The shift of phonon modes to lower frequency with decreasing size or dimension may be explained by the increasing surface-to-volume ratio or the decreasing bonding force acting on the surface atoms. The modified phonon properties and the shifted population distribution must change the PBTE solutions quantitatively.

The confined phonon density of states is also important as far as the temperature quantum correction is concerned. The corrected temperature (T) is related to the classical one T_{MD} by

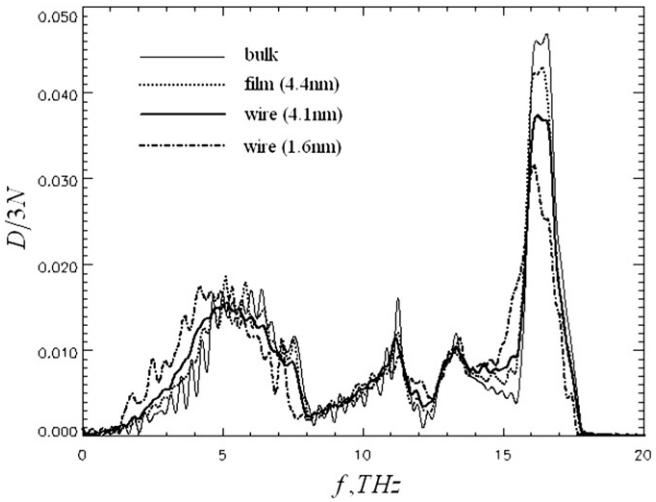

Fig. 4. The normalized phonon density of states, $D/3N$.

$$3Nk_BT_{MD} = \int_0^{\omega_D} D(\omega)[n(\omega,T) + 1/2]\hbar\omega d\omega \tag{3}$$

where $n(\omega,T) = (\exp(\hbar\omega/k_BT) - 1)^{-1}$ is the equilibrium phonon distribution and ω_D is the Debye frequency. Equation (3) equates the system energy from the quantum description to the simulated one [26]. Note some previous investigations did not include the zero-point energy $\hbar\omega/2$ in the formula [24,25] in order to have a null energy at 0K like the classical definition. A nearly constant difference between T and T_{MD} for a given system energy is nonetheless resulted when the temperature is high. Because we are interested in room-temperature applications, the zero-point energy is taken into consideration in the present study. The corrected results according to Eq. (3) based on the Debye-model [24,25], bulk, thin film, and wire densities of states are all shown together in Fig. 5. As seen, the corrected temperatures based on the computed densities of states are nearly all the same, regardless of the dimension and the film/wire thickness (the latter is not shown herein), except at very low temperature. The difference between them and the Debye result is however distinguishable. We thus conclude in performing the temperature quantum correction, the

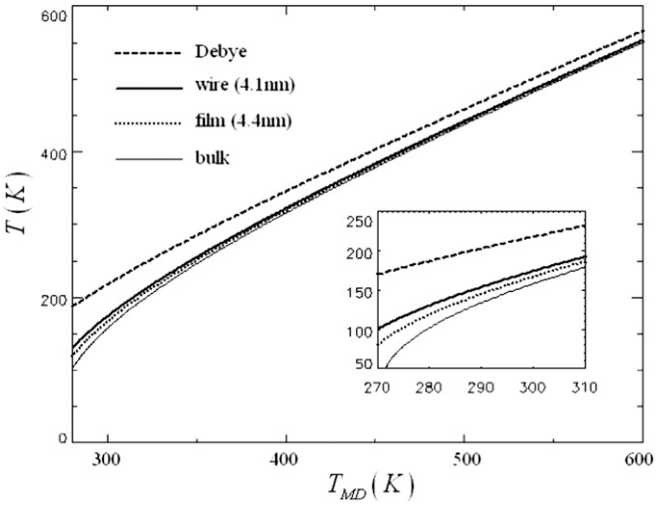

Fig. 5. A comparison of the quantum corrected temperatures based on the Debye-model, bulk, film, and wire phonon densities of states.

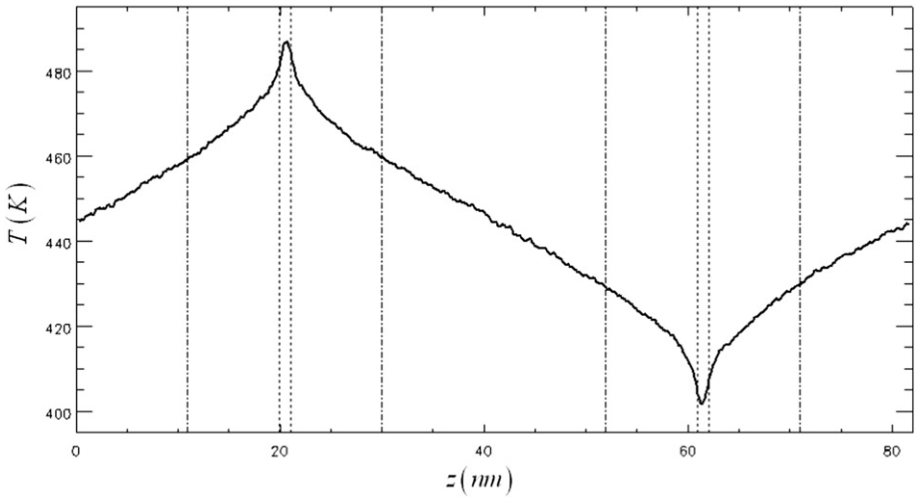

Fig. 6. The temperature distribution along the axis of the silicon wire having a diameter of 7.6 nm and a length of 82 nm with $\Delta\varepsilon/A = 0.1$ meV/nm^2. The narrow regions bracketed by the dotted lines are the energy source and sink regions.

bulk density of states is acceptable for low-dimensional materials but the Debye-model one is not.

3.2. Axial thermal conductivity

Besides the confined phonon spectra, we also calculate the thermal conductivity of silicon nanowires in the present study. The simulation is first run for 55 ps ($\Delta t = 0.55$ fs) by enforcing the whole system at a prescribed temperature. The energy addition and extraction mechanism is then actuated and the simulation is run for another 660 ps for the non-equilibrium system to reach stationary. Statistical samples are then taken. Fig. 6 shows the averaged temperature distribution over 990 ps for the silicon wire of diameter 7.6 nm and length 82 nm. Note all the temperatures have been quantum corrected by using the confined phonon density of states of the silicon wire. By truncating the nonlinear part of the temperature distribution (bracketed by the dash dotted lines), which arises from the strong scattering in the energy source and sink regions, we take the remaining linear part and the imposed heat flux to calculate the thermal conductivity.

Such a thermal conductivity is however not the thermal conductivity of an infinitely long wire due to the numerical finite-size effect; in other words, the wave length of the lattice vibration that can be excited is limited by the simulated wire length L_z. To fix it, we adopt the extrapolation strategy suggested by Schelling et al. [27]. Based on the belief that the inverse of the thermal conductivity (k) is linearly related to the inverse of the simulated wire length, several lengths are first simulated and the thermal conductivity of the infinitely long wire is then extrapolated by letting $1/L_z \to 0$. The linear dependence of $1/k$ on $1/L_z$ is confirmed in all wires and temperatures simulated herein. Fig. 7 illustrates the results at $T_{MD} = 400$ K.

The temperature dependence of the thermal conductivity of infinitely long silicon wires is now shown in Fig. 8, compared with that of infinite silicon thin films. It is seen the thermal conductivity

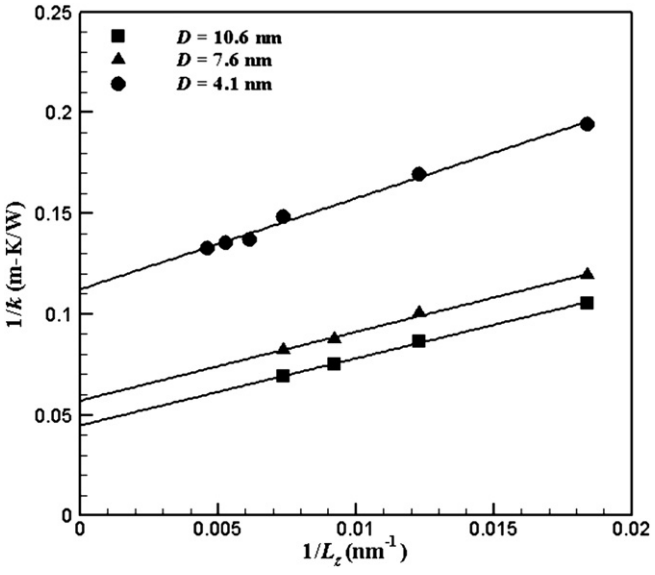

Fig. 7. The linear dependence of $1/k$ on $1/L_z$ at $T_{MD} = 400$ K.

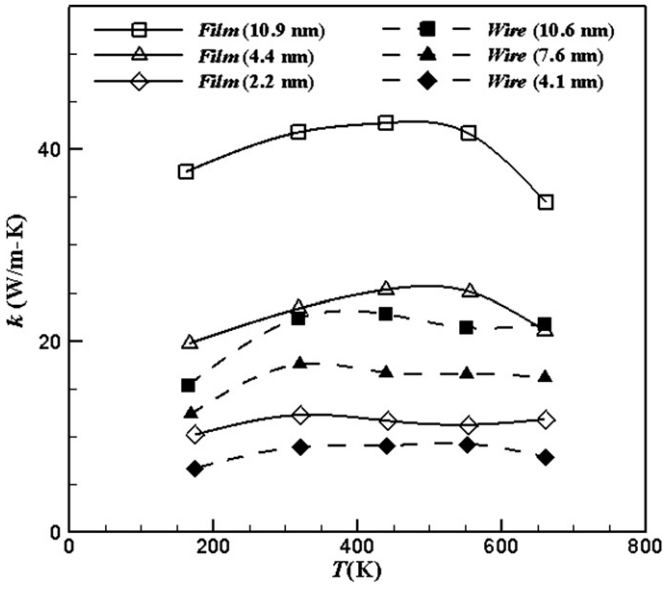

Fig. 8. The temperature dependence of the thermal conductivities of infinitely long silicon wires compared to those of infinite thin films.

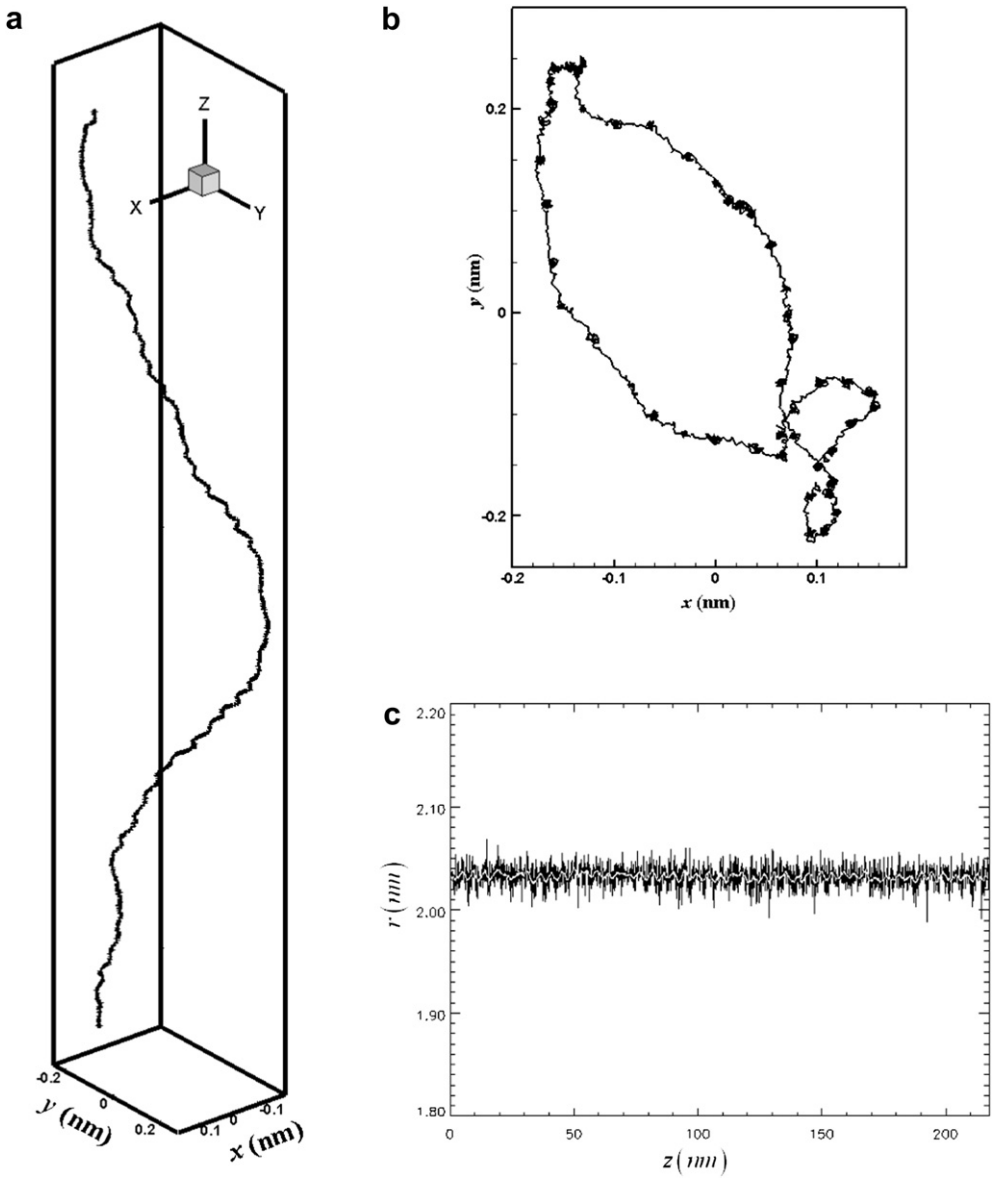

Fig. 9. The curved axis and radius of the silicon wire of diameter 4.1 nm and length 217 nm at 700 K: (a) a 3D illustration (x:y:z = 1:1:80); (b) top view of (a); (c) the local radius.

decreases with the decreasing film/wire thickness due to the increasing surface scattering and the reduced phonon group velocity. Their dependence on the temperature is not strong, although a little bump can be found carefully. Finally, the thermal conductivity of the wire is about half that of the thin film for a same thickness.

The present simulation results are quantitatively different from those obtained by Ponomareva et al. [38], who investigated the thermal conductivities of silicon tetrahedral and clathrate nanowires with diameters in the range of 1.4–8.3 nm using the NEMD approach. The thermal conductivity of tetrahedral wires they found is about 20 W/m K at 300 K. Their wires had a finite length and their temperatures were not quantum corrected. These might explain the difference.

At last, it is worth examining the straightness and thickness uniformity of the simulated wires because these effects can influence the thermal conductivity as well. We compute the average cross-sectional coordinates $(\overline{x}, \overline{y})$ of atoms in each slice and define it as the location of the wire axis at the middle z-coordinate of the slice. The average projected distance on the x–y plane of the surface atoms from it is then defined as the local radius of the wire. We show in Fig. 9 the results of the silicon wire of diameter 4.1 nm and length 217 nm at 700 K (the thinnest and longest wire at the highest simulated temperature). To reduce the statistical noise, a fifteen-point local smoothing has been applied to Fig. 9(a),(b), and the white curve in Fig. 9(c). The variation in the radius is little (under 2%) and the deviation of the wire axis from a perfect straight line is about 10% of the diameter but only 0.2% of the wire length. The influence of the curved axis on the thermal conductivity is thus expected to be negligible in all cases studied in the present work.

4. Conclusion

We investigate the confined phonon dispersion relations and densities of states of silicon nanowires in use of the equilibrium molecular dynamics approach. These phonon properties are very important in obtaining accurate solutions of the phonon Boltzmann transport equation. The simulation results show that, besides discrete

acoustic phonon modes accompanied with smaller group velocities, many additional modes are excited in the region of large wave numbers and small frequencies, resulting in a shifted distribution of the phonon density of states. This is explained by the decreasing bonding force acting on the surface atoms. The lattice thermal conductivities of silicon wires of diameter 4.1 nm, 7.6 nm, and 10.6 nm are also calculated using the non-equilibrium molecular dynamics simulation. The temperature quantum correction is done based on the confined phonon density of states and the extrapolation technique is employed to eliminate the numerical finite-size error. It is found the lattice thermal conductivities of silicon nanowires are largely reduced due to the surface scattering and the confined, smaller, phonon group velocity and depend only weakly on the temperature, implying a dominance of the surface scattering over the phonon–phonon interaction.

Acknowledgement

This work was supported by the Industrial Technology Research Institute of Taiwan, R.O.C (project No. 97-S-A36) as well as by the National Science Council of Taiwan (Grant No. NSC 97-2221-E-002-200-MY3). We are also grateful to Computer and Information Networking Center, National Taiwan University, and the National Center for High-performance Computing for the support of high-performance computing facilities.

References

[1] R. Venkatasubramanian, E. Siivola, T. Colpitts, B. O'Quinn, Thin-film thermoelectric devices with high room-temperature figures of merit. Nature 413 (2001) 597–602.
[2] D.G. Cahilla, W.K. Ford, K.E. Goodson, G.D. Mahan, A. Majumdar, H.J. Maris, R. Merlin, S.R. Phillpot, Nanoscale thermal transport. J. Appl. Phys. 93 (2003) 793–818.
[3] J.P. Heremans, Low-dimensional thermoelectricity. Acta Phy. Pol. A 108 (2005) 609–634.
[4] L.D. Hicks, M.S. Dresselhaus, Thermoelectric figure of merit of a one-dimensional conductor. Phys. Rev. B 47 (1993) 16631–16634.
[5] L.D. Hicks, M.S. Dresselhaus, Effect of quantum-well structures on the thermoelectric figure of merit. Phys. Rev. B 47 (1993) 12727–12731.
[6] A. Khitun, A. Balandin, K.L. Wang, Modification of the lattice thermal conductivity in silicon quantum wires due to spatial confinement of acoustic phonons. Superlattices Microstruct. 26 (1999) 181–193.
[7] M.J. Huang, W.Y. Chong, T.M. Chang, The lattice thermal conductivity of a semiconductor nanowire. J. Appl. Phys. 99 (2006) 114318.
[8] M.J. Huang, T.M. Chang, W.Y. Chong, C.K. Liu, C.K. Yu, A new lattice thermal conductivity model of a thin film semiconductor. Int. J. Heat and Mass Transf. 50 (2007) 67–74.
[9] J. Heremans, C.M. Thrush, Y. Lin, S. Cronin, Z. Zhang, M.S. Dresselhaus, J.F. Mansfield, Bismuth nanowire arrays: synthesis and galvanomagnetic properties. Phys. Rev. B 61 (2000) 2921–2930.
[10] J.P. Heremans, C.M. Thrush, D.T. Morelli, M. Wu, Thermoelectric power of bismuth nanocomposites. Phys. Rev. Lett. 88 (2002) 216801.
[11] J. Lee, S. Farhangfar, J. Lee, L. Cagnon, R. Scholz, U. Gosele, K. Nielsch, Tuning the crystallinity of thermoelectric Bi2Te3 nanowire arrays grown by pulsed electrodeposition. Nanotechnology 19 (2008) 365701.
[12] Y. Lin, X. Sun, M.S. Dresselhaus, Theoretical investigation of thermoelectric transport properties of cylindrical Bi nanowires. Phys. Rev. B 62 (2000) 4610–4623.
[13] D. Li, Y. Wu, P. Kim, L. Shi, P. Yang, A. Majumdar, Thermal conductivity of individual silicon nanowires. Appl. Phys. Lett. 83 (2003) 2934–2936.
[14] A.R. Abramson, W.C. Kim, S.T. Huxtable, H. Yan, Y. Wu, A. Majumdar, C.L. Tien, P. Yang, Fabrication and characterization of nanowire/polymer-based nanocomposite for a prototype thermoelectric device. J. MEMS 13 (2004) 505–515.
[15] J.H. Seol, A.L. Moore, S.K. Saha, F. Zhou, L. Shi, Q.L. Ye, R. Scheffler, N. Mingo, T. Yamada, Measurement and analysis of thermopower and electrical conductivity of an indium antimonide nanowire from a vapor–liquid–solid method. J. Appl. Phys. 101 (2007) 023706.
[16] J. Zou, A. Balandin, Phonon heat conduction in a semiconductor nanowire. J. Appl. Phys. 89 (2001) 2932–2938.
[17] P. Hyldgaard, G.D. Mahan, Phonon Knudsen flow in GaAs/AlAs superlattices. Proc. 23rd Int. Thermal Conduct. Conf. 23 (1996) 172–182.
[18] S.G. Walkauskas, D.A. Broido, K.K. Kempa, T.L. Reinecke, Lattice thermal conductivity of wires. J. Appl. Phys. 85 (1999) 2579–2582.
[19] S. Mazumder, A. Majumdar, Monte Carlo study of phonon transport in solid thin films including dispersion and polarization. J. Heat Transf. 123 (2001) 749–759.
[20] D. Lacroix, K. Joulain, D. Lemonnier, Monte Carlo transient phonon transport in silicon and germanium at nanoscale. Phys. Rev. B 72 (2005) 064305.
[21] R.B. Peterson, Direct simulation of phonon-mediated heat transfer in a Debye crystal. J. Heat Transf. 116 (1994) 815–822.
[22] M.J. Huang, T.C. Tsai, L.C. Liu, M.S. Jeng, C.C. Yang, A fast Monte-Carlo solver for phonon transport in nanostructured semiconductors. CMES 42 (2009) 107–129.
[23] J.M. Dickey, A. Paskin, Computer simulation of the lattice dynamics of solids. Phys. Rev. 188 (1969) 1407–1418.
[24] X.L. Feng, Z.X. Li, Z.Y. Guo, Molecular dynamics simulation of thermal conductivity of nanoscale thin silicon films. Microscale Thermophys. Eng. 7 (2003) 153–161.
[25] Wang Zeng-hui, Li Zhixin, Research on the out-of-plane thermal conductivity of nanometer silicon film. Thin Solid Films 515 (2006) 2203–2206.
[26] C.J. Gomes, M. Madrid, J.V. Goicochea, C.H. Amon, In-plane and out-of-plane thermal conductivity of silicon thin films predicted by molecular dynamics. J. Heat Transf. 128 (2006) 1114–1121.
[27] P.K. Schelling, S.R. Phillpot, P. Keblinski, Comparison of atomic-level simulation methods for computing thermal conductivity. Phys. Rev. B 65 (2002) 144306.
[28] S. Plimpton, Fast parallel algorithms for short-range molecular dynamics. J. Comput. Phys. 117 (1995) 1–19.
[29] P. Heino, Dispersion and thermal resistivity in silicon nanofilms by molecular dynamics. Eur. Phys. J. B 60 (2007) 171–179.
[30] C. Flensburg, R.F. Stewart, Lattice dynamical Debye–Waller factor for silicon. Phys. Rev. B 60 (1999) 284–291.
[31] P. Jund, R. Jullien, Molecular-dynamics calculation of the thermal conductivity of vitreous silica. Phys. Rev. B 59 (1999) 13707–13711.
[32] M.P. Allen, D.J. Tildesley, Computer Simulation of Liquids. Oxford, 1987.
[33] V.Y. Trubitsyn, E.B. Dolgusheva, Molecular dynamics calculations of anharmonic properties of the vibrational spectrum of BCC zirconium under pressure. Phys. Solid State 49 (2007) 1345–1352.
[34] N.I. Papanicolaou, I.E. Lagaris, G.A. Evangelakis, Modification of phonon spectral densities of the (100) copper surface due to copper adatoms by molecular dynamics simulation. Surf. Sci. 337 (1995) 819–824.
[35] L.J. Porter, J.F. Justo, S. Yip, The importance of Grueisen parameters in developing interatomic potentials. J. Appl. Phys. 82 (1997) 5378–5381.
[36] W. Weber, Adiabatic bond charge model for the phonon in diamond, Si, Ge, and (alpha)-Sn. Phys. Rev. B 15 (1977) 4789–4803.
[37] G. Nilsson, G. Nelin, Study of the homology between silicon and germanium by thermal-neutron spectrometry. Phys. Rev. B 6 (1972) 3777–3786.
[38] I. Ponomareva, D. Srivastava, M. Menon, Thermal conductivity in thin silicon nanowires: phonon confinement effect. Nano Lett. 7 (2007) 1155–1159.